Open access • Journal Article • DOI:10.1051/EPJAP/2021200217

An ab initio investigation of the electronic and magnetic properties of graphite and nickel-doped graphite — Source link

Abdellah Sellam, E.K. Hlil, Rodolphe Heyd, Abdelaziz Koumina

Institutions: Cadi Ayyad University, University of Grenoble, ParisTech

Published on: 01 Apr 2021 - European Physical Journal-applied Physics (EDP Sciences)

Topics: Coherent potential approximation, Magnetism, Density of states, Magnetic moment and Graphite

Eur. Phys. J. Appl. Phys. **94**, 10401 (2021)

https://doi.org/10.1051/epjap/2021200217

THE EUROPEAN PHYSICAL JOURNAL APPLIED PHYSICS

Regular Article

An ab initio investigation of the electronic and magnetic properties of graphite and nickel-doped graphite

Abdellah Sellam[1,*], El Kebir Hlil[2], Rodolphe Heyd[3], and Abdelaziz Koumina[4]

[1] ENS, Cadi Ayyad University, Marrakech, Morocco
[2] Univ. Grenoble Alpes, CNRS, Grenoble INP, Institut Neel, 38000 Grenoble, France
[3] Angevin Laboratory of Mechanics, Processes and InnovAtion (ALMPI). ENSAM ParisTech, Angers, France
[4] ENS, Cadi Ayyad University, Marrakech, Morocco

Received: 6 July 2020 / Received in final form: 3 January 2021 / Accepted: 4 March 2021

Abstract. In this paper, the KKR (Korringa, Kohn, and Rostoker) is presented with coherent potential approximation methods which is used to investigate the electronic and magnetic properties of allotropic graphite forms of carbon and nickel-doped graphite. The density of states (DOS), band structure, total energy, and the magnetic moments of atoms are computed. The crystallographic structure optimization is carried out by evaluating the total energy as a function of unit lattice parameters. The DOS analysis reveals a partially metallic behavior of the compound. The magnetism vs the Ni-doping content in $C_{1-x}Ni_x$ is also investigated by computing moments induced on atoms; the sensitivity of the magnetism to Ni-doping is also analyzed.

1 Introduction

Graphite is a stable form of carbon at a room temperature and under ambient pressure. It manifests a semi metallic state that has been systematically investigated due to its potential use in the technological and to its archetypal bi-dimensional properties. The study of graphite intercalation compound (GIC) is closely linked to the nature of the interlayer binding. The crystal structure of the graphite is a planar hexagonal network showing layers that generally adopt an ABAB$\cdots$ piling sequence (Bernal structure, Fig. 1b). The natural and the synthesized crystalline graphite is a mixture of Bernal and rhombohedral graphite where the layers are piled in an ABCABC pattern, with proportions of 80% Bernal, 14% rhombohedral, and 6% disordered graphite. In (GIC) structure, the layers of carbon can be piled in various ways, either similar to the Bernal structure (ABAB$\cdots$ stacking), or with layers of carbon atoms located directly in a pile like structure (AAA$\cdots$ stacking). These two modifications of graphite are illustrated in Figure 1. In disordered or pregraphite Carbon typically called turbostratic graphite, the Carbon atoms are in a consecutive layers directly above one another. This configuration of simple hexagonal graphite has not been observed in crystalline graphite. All previous calculations have been focused on the structural and electronic properties of the stressed graphite having the Bernal or rhombohedral structure. In this paper, an ab initio calculations were performed in order to investigate the electronic and magnetic properties. The band structure, DOS, total energy and magnetic moments are computed. For the structural optimization of volume, then the ratio (c/a), the optimization procedure is used reported in reference [1]. The procedure was repeated iteratively in order to obtain the lattice parameters of the proposed structure whith 0.001 bohr as precision. Such optimisation, based on the functional theory of density [2,3] using linearized augmented plane waves plus orbitals (LAPW + lo) [4], were implemented in the Wien2K code [5]. The calculations involved both the local density approximation (LDA) [6] and the generalized gradient approximation (GGA) [7]. The results are gathered in Tables 1 and 2.

In 1924, Bernal reported graphite as a set of parallel hexagonal sheets of carbon atoms arranged in an AB stacking pattern [8]. Later, Wyckoff [9] reviewed graphite using the lattice parameters mentioned by Baskin and Mayer, $a = 0.246$ nm and $c = 0.667$ nm [10].

2 Calculation methods

2.1 The Korringa, Kohn, and Rostoker method with coherent potential approximation

The Korringa, Kohn, and Rostoker (KKR) method [11,12] was used to calculate the electronic band structure and the electronic DOS within the coherent potential approximation (CPA) [13,14].

This method was used by Akai and Dederichs for the treatment of transition metal alloys [15], with the parameterization of Vosko, Wilk and Nusair (VWN). We used the MACHIKANEYAMA2002V10 code produced by Akai [16]. The Local Density Approximation (LDA) is the most widely used approximation in the functional density theory (DFT) [17]. The Green function technique is employed to solve the Schrödinger equation, without resorting to

* e-mail: selamabdo1976@hotmail.com

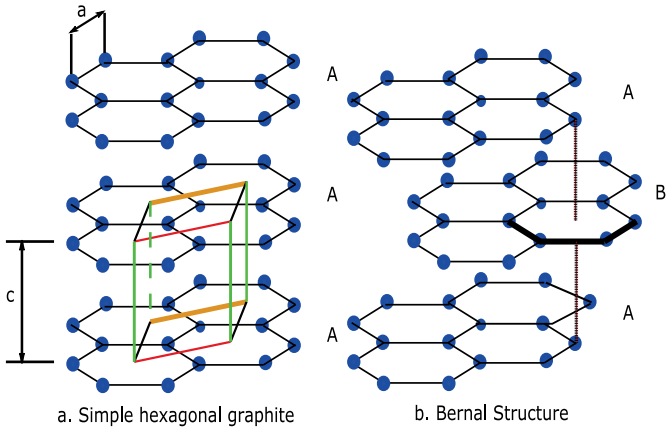

Fig. 1. Different graphitic stackings: simple hexagonal graphite (a) and natural hexagonal graphite (Bernal structure) (b) are displayed. They differ in the shift of the middle plane in the ABA stacking (all planes are directly above each other in the AAA stacking). The unit cell of the simple hexagonal crystalline structure is also shown. The interlayer distance is c and the distance between the nearest neighbors is a [18].

Table 1. Graphite AB: spatial group 194 ($P6_3/mmc$).

	LDA	GGA	Exp [4,8]
a (pm)	244.7	246.8	246.0
c (pm)	656.5	922.9	667
c/a	2.720	3.739	2.73
Total energy (Ry)	−302.5	−304.8	−−

Table 2. Graphite AA: spatial group 191 ($P6/mmm$).

	LDA	GGA
a (pm)	244.7	246.9
c (pm)	360.1	477.2
c/a	1.471	1.933
Total energy (Ry)	−151.2	−152.4

the explicit calculation of the wave functions and eigenvalues of the Hamiltonian system. In this approach, the scattering properties of each diffusion center (atom) are described by a scattering matrix, whereas multiple scattering by all the atoms in the lattice is determined by considering that the incident wave at each center is the sum of the outgoing waves from other scattering centers.

2.2 The Green's function method

Let H be the Hamiltonian of an electron in the system then, the Green's operator G is defined [19,20]:

$$G = \lim_{\eta \to 0^+} \frac{1}{E - H + \mathrm{i}\eta} \tag{1}$$

where η is a positive real number and i is the imaginary unit. If $|k\rangle$ and $|k'\rangle$ represent two eigenvectors of H, then:

$$\langle k|G|k'\rangle = \delta_{k,k'} \lim_{\eta \to 0^+} \frac{1}{E - E_k + i\eta} \tag{2}$$

where E_k is the eigenvalue associated with $|k\rangle$ and $\delta_{k,k'}$ is the Kronecker symbol. Accordingly, G can be redefined as follows using projectors:

$$G = \lim_{\eta \to 0^+} \sum_k \frac{|k\rangle\langle k|}{E - E_k + i\eta}. \tag{3}$$

The trace of operator G, denoted by $\mathrm{Tr}\, G$, is given by:

$$\mathrm{Tr}\, G = \sum_k \lim_{\eta \to 0^+} \frac{1}{E - E_k + i\eta}. \tag{4}$$

It was shown [19,20] that the imaginary part of the Green operator trace, $\mathrm{Im\,Tr}G$, was related to the electronic states density $n(E)$ based on the following relationship:

$$n(E) = -\frac{1}{\pi} \mathrm{Im\,Tr}\, G. \tag{5}$$

This relationship is particularly interesting since the G trace is invariant, and the G matrix can be determined in any form of the representation.

Another useful expression of the DOS is deduced from the following elementary relation:

$$\frac{1}{E - E_k + i\eta} = -\frac{\mathrm{d}}{\mathrm{d}E} \ln\left(\frac{1}{E - E_k + i\eta}\right). \tag{6}$$

In a representation where the matrix of G is diagonal, we have:

$$\frac{\mathrm{d}}{\mathrm{d}E} \ln(\det G) = -\sum_k \frac{1}{E - E_k + i\eta}. \tag{7}$$

Then, it follows that:

$$n(E) = \frac{1}{\pi} \frac{\mathrm{d}}{\mathrm{d}E} \mathrm{Im}\, \ln(\det G). \tag{8}$$

If we express $n(E)$ in an atomic orbital base $\{\varphi_p\}$, where the index p can include an atomic position in the crystal and a spin index s, we can then deduce that:

$$n(E) = -\frac{1}{\pi} \mathrm{Im\,Tr}\, G = -\frac{1}{\pi} \mathrm{Im} \sum_p \langle \varphi_p|G|\varphi_p\rangle. \tag{9}$$

Let's substitute the mathematical expression of G with:

$$G = \lim_{\eta \to 0^+} \sum_k \frac{|k\rangle\langle k|}{E - E_k + i\eta}. \tag{10}$$

Then we obtain:

$$n(E) = -\frac{1}{\pi} \mathrm{Im} \sum_{p,k} \frac{|\langle \varphi_p|G|\varphi_p\rangle|^2}{E - E_k + i\eta}. \tag{11}$$

As a result:

$$\mathrm{Im} \frac{1}{E - E_k + i\eta} = -\pi\delta(E - E_k). \tag{12}$$

Then, equation (11) becomes:

$$n(E) = \sum_{p,k} |\langle \varphi_p|G|\varphi_p\rangle|^2 \delta(E - E_k). \tag{13}$$

Defining the local DOS:

$$n_p(E) = \sum_k |\langle\varphi_p|G|\varphi_p\rangle|^2 \delta(E - E_k) \tag{14}$$

where p is an atom index, we obtain:

$$n(E) = \sum_p n_p(E). \tag{15}$$

Consequently, the contribution of any state of energy E_k to $n(E)$ is weighted by the orbital weight φ_p. Therefore, $n_p(E)$ represents the contribution of φ_p to the total DOS $n(E)$.

It can be seen from previous relations that the calculation of DOS the requires knowledge of the Green's operator G. In the present work, this was done using the KKR-CPA approach, taking into account multiple-sites scattering within the muffin-tin approximation.

3 The atomic properties and graphitic structure and Ni-doping on graphite

3.1 The atomic properties and graphitic structure

The configuration of the ground state of carbon atoms is $1s^2 2s^2 2p^2$ [21]. The core electrons are in the first orbital $1s^2$ and the remaining four electrons take place at the valence band. The energies of the $2s$ and $2p$ levels are respectively at -13 and -5 eV below the vacuum level. The $1s$ level is well below and appears at -35 eV [22].

Inside the core shell no p electrons is found. Due to the orthogonalization with the core state [23], the p valence electrons did not come under the impact of repulsion. The $2p$ wave function is quite localized [22]. The distance to the nucleus of the orbital $2p$ wave-function maximum is almost the same as the orbital $2s$ wave-function maximum. In both allotropic forms which are the diamond and the graphite we can find natural carbon. The bonding between atoms is different in each form, but are mainly covalent. In diamond, the bonds arise from the sp^3 hybridization of atomic orbitales four bonds and angles of 109.5°.

In graphite, the sp^2 $(s - p_x - p_y)$ hybridization of atomic orbitales (denoted σ) formed a covalently bound lattice of graphitic planes with angles of 120° between the bounds connecting adjacent atoms to neighbor atoms, They are stacked one on top of the other and weakly bounded by the residual forces that arose from the non-hybridized p_z orbitales (denoted as π) perpendicular to the planes. The graphitic lattice (c) and the three-dimensional Brillouin zones (d) are shown in Figure 2.

In a graphitic monolayer, the first four bands (σ and π) are occupied and the last four are empty. Because of symmetrical properties, π (bonding) and π^* (antibonding) bands degenerated at the K point of the two dimensional ($2D$) Brillouin zones. As result, the ($2D$) graphite is a zero-gap semiconductor [21]. This situation is modified by interactions between graphitic planes and semi-metal is created. However, these weak interactions could be considered as perturbations of the $2D$ situation.

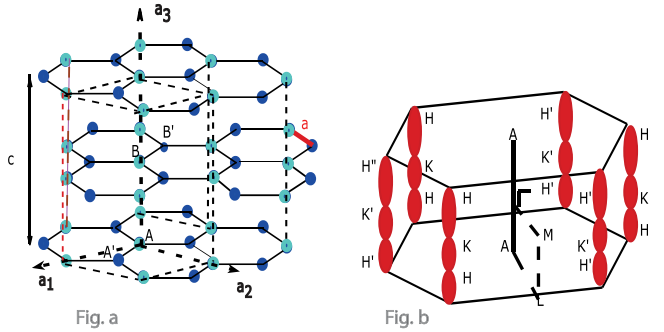

Fig. 2. (a) Crystalline structure of the hexagonal graphite [21]. The parameters of the unit cell, represented by dotted-dashed lines, are a_1, a_2 and $a_3 = c$. a is the distance between nearest neighbours; (b) graphite Brillouin zone showing several high-symmetry points. A schematic version of the graphite electron and hole Fermi surfaces located along the $H - K$ axes [21,24]. Each symmetric point is labeled with the usual Bouckaert-Smoluchowski-signer notation (Γ, A, H, K, L, M).

The $3D$ structure of graphite is not a straightforward piling of planes. Instead, every other plane is moved in the horizontal plane to create the ABABAB piling pattern as displayed in Figure 2c.

The $P6_3/mmc$ space group contains the crystallographic structure. Four atoms exist in the $3D$ unit cell: two atoms for each graphitic plane and two planes per cell (AB) displayed in Figure 2c. Also, this figures presents the cell, which is high and narrow.

At $0K$, the lattice parameters are $c = 0.066$ nm and $a = 0.024$ nm [25]. From this, the distance between planes 0.033 nm and between nearest neighbours 0.014 nm [21] were estimated.

3.2 Ni-doping on graphite

Nickel doping has attracted attention due to its basic magnetic properties, which it is hoped to confer to graphene/graphite through doping. It is a long tradition in the graphite field and graphite intercalation compounds (GIC), to take advantage of the large interplane distances of graphene (and thus the weakest bonds/interactions) to try to introduce elements of another nature, to change its physical properties. It is reasonable today, with the available numerical computation methods (KKR, GPAW ...), to start with a simulation (fast and inexpensive) rather than an experiment that requires complex synthesis and analysis equipment, not necessarily available in all laboratories. This is also quoted in article [26].

4 Results and discussion

4.1 Optimization of the graphite structure

The structural optimizations for graphite were based on the KKR-CPA calculations of the total energy of the graphite system as a function of the (c/a) ratio. The equilibrium parameters corresponded to the calculated minimum energies. Figure 3 shows that these optimized

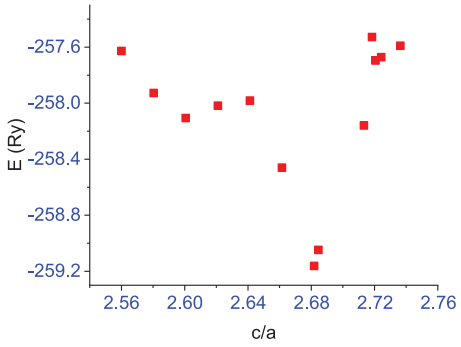

Fig. 3. Mesh parameters optimization $E(Ry)$ according to (c/a). In our KKR calculations to look for energy optimization by varying the (c/a) ratio, we started the calculation from the experimental value $(c/a = 2.73)$ cited in references [4,8] and when this value decreased, we observe a minimum in $(c/a = 2.682)$, then we continued the calculation with a step of $(c/a = 0.020)$.

parameters indicate a minimum value for:

$$\frac{c}{a} = 2.682.$$

4.2 Density of state according to the ratio (c/a)

To investigate the effect of the (c/a) parameter of graphite on DOS, the following data are used:

- the pure compound is the graphite carbon with hexagonal structure.
- The mesh parameters found by optimization in the previous sect. **(4.1)** are $a = 0.246$ nm and $c = 0.660$ nm.
- To improve the quality of our calculations, we added eight empty spheres (ES) with $Z = 0$ at the intersites of the four carbon atoms.
- The positions of the carbon graphite are: C1 (0a 0b 0c), C2 (1/3a 2/3b 0c), C3 (0a 0b 1/2c) and C4 (2/3a 1/3b 1/2c).
- The positions of the eight empty spheres (ES) are: Vc1 (2/3a 1/3b 0c), Vc2 (0a 0b 1/4c), Vc3 (1/3a 2/3b 1/4c), Vc4 (2/3a 1/3b 1/4c), Vc5 (1/3a 2/3b 1/2c), Vc6 (0a 0b 3/4c), Vc7 (1/3a 2/3b 3/4c) and Vc8 (2/3a 1/3b 3/4c).
- The quality of the Brillouin Zone mesh is chosen in the settings of the input file of the KKR calculation as follows: bzqlty = 4.

Firstly, comparing the DOS of the graphite from our calculations to the DOS reported in reference [27], we find that there is a strong consistency between both calculations. Our investigation points out to the following results: The effect of the graphite parameter (c/a) on DOS is shown in Figures 5–7 (see also Figs. A.1-A.4), while retaining the same values of parameters edelt and ewidth parameters whose meanings are given in Figure 7. Moreover, an energy resonance is observed at $(c/a = 2.720)$ Figure 8, where the DOS decreased significantly in the

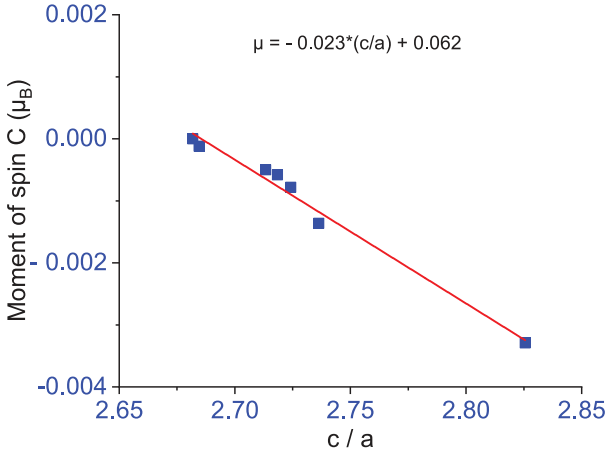

Fig. 4. The spin moment variation versus the (c/a) ratio. The spin moment showed a linear dependence of the change in (c/a) ratio ranging from 2.682 to 2.826.

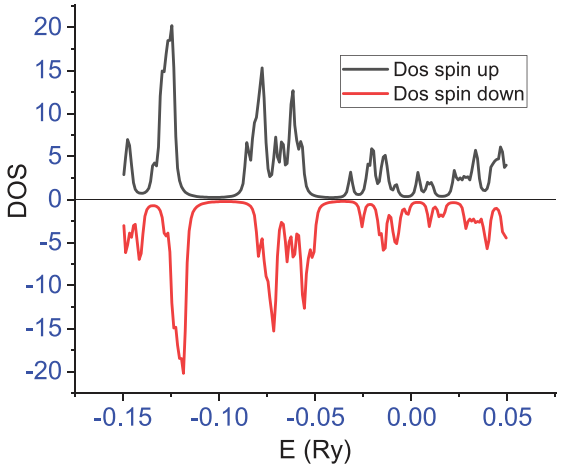

Fig. 5. The DOS computed for the parameter $(c/a = 2.682)$ which corresponds to minimal energy in the optimization of the structure on the graphite DOS.

vicinity of the Fermi energy. Contrarily, when the (c/a) ratio changes, the density varies in vicinity of the Fermi energy. The symmetry of the spin-up and spin-down density shifted with respect to the energy axis by 0.006 Ry, depending on the value of (c/a) Figure 6. The calculated DOS evidenced that the graphite always indicated a semimetallic character, regardless of the value of the (c/a) ratio. In addition, spin momentum displayed in Figure 4 revealed a linear dependence on the variation of (c/a) ratio ranging from 2.682 to 2.826.

$$\mu(spin\ momentum)(\mu_B) = -0.023 \times (\frac{c}{a}) + 0.062.$$

4.3 The doping of graphite by nickel

4.3.1 Atomic properties and nickel structure

Nickel, belongs is the space group Fm-3m(225) and its cell parameter equal to 0.352 nm. It possesses an

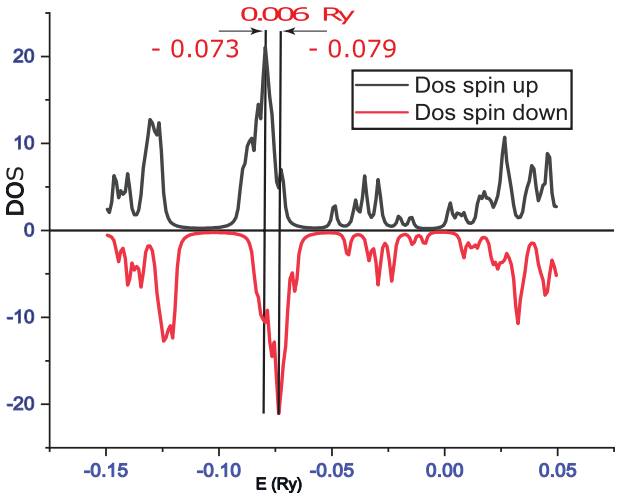

Fig. 6. The DOS computed for the parameter ($c/a = 2.713$). On the DOS of the graphite and which shows that the symmetry of the spin-up and spin-down density shifted with respect to the energy axis by $0.006Ry$, as a function of the (c/a) value.

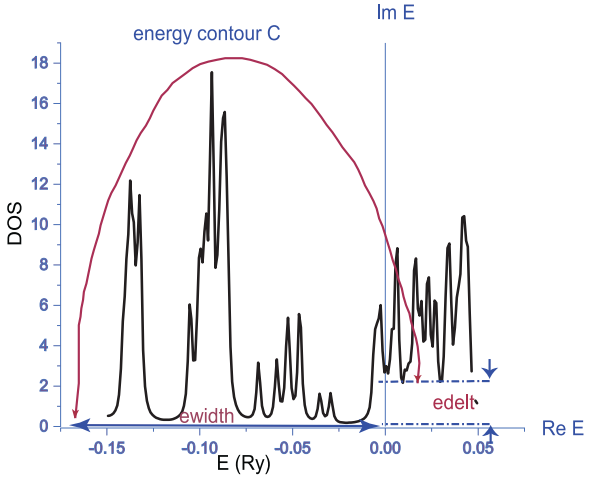

Fig. 7. Both parameters edelt and ewidth displayed on the DOS curve. The edelt is imaginary part of energy in the vicinity of Fermi level. The ewidth represents width of the energy contour in Ry.

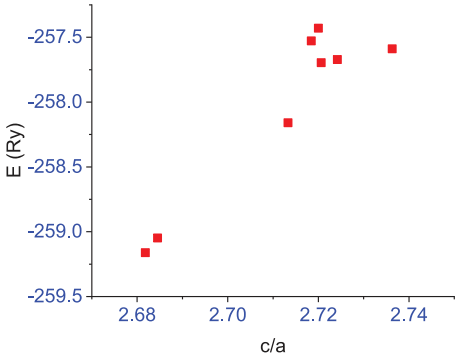

Fig. 8. The variation of energy as a function of (c/a) and the resonance phenomenon which corresponds to the value ($c/a = 2.720$).

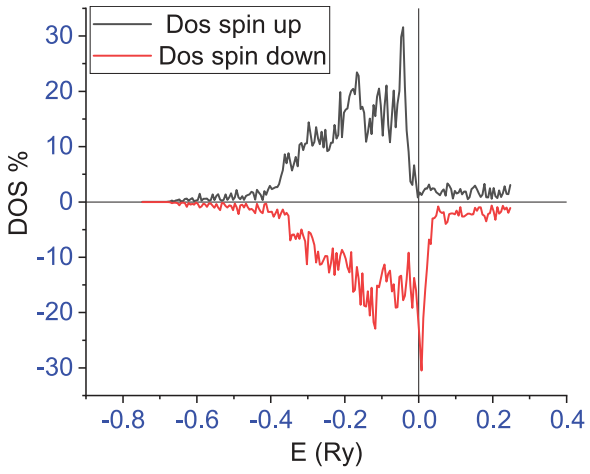

Fig. 9. Density of states versus energy of Nickel. Calculations are performed using space group $Fm-3m$ (225) and cell parameter equal to $a = 0.352$ nm.

atomic number $Z = 28$ and an electronic configurations $[Ar]3d^8 4s^2$.

From calculations, we observed an asymmetry of both state densities of spin up and down with respect to the energy axis. It indicates a magnetic state for Ni. The Fermi level taken as energy reference is represented by the vertical line ($E = 0$ Ry).

The computed magnetic moment is equal to $0.63\,\mu_B$ [12]. In addition, our computed DOS displayed in Figure 9 is perfectly superposable with the DOS reported in reference [12].

4.3.2 Nickel-doping on graphite

In this section, we present the effect of nickel-doping on the graphite properties. Precisely, we analyzed the changes in total energy, in the DOS, and in the magnetic moment carried by atoms vs Ni content. The calculated DOS for different Ni concentrations, in $C_{1-x}Ni_x$ system, are reported in Figures 10 and 11 (see also Figs. B.1-B.4). The symmetry with the respect to energy axis was clearly observed between the electrons of the majority spins and those of the minority spins, which permitted the assertion that the $C_{x-1}Ni_x$ was a non-magnetic material. Comparing the DOS calculated for graphite and Ni-doped graphite, we find that they are somewhat similar for the majority and minority spins. However there are unoccupied states in the $C_{x-1}Ni_x$ system taking place at high energies. This unoccupied state corresponds to the addition of two Ni valence electrons. The total energy and the spin moment based on the x concentration are presented as well. Here, we underline that the NiC alloy on which the calculation were performed exists and was already synthesized and related experimental results have been previously reported by Cadeville et al. [28]. They claimed that the solubility of Carbone in Ni achieved by quenching of the liquid state at 293 K (at.−%) is equal to 1.5. Also, they report that the variation of the mesh parameters $(da/dc)(10^{-4}\,\text{nm/at.}-\%)$ equal to 7.6 [28]. In

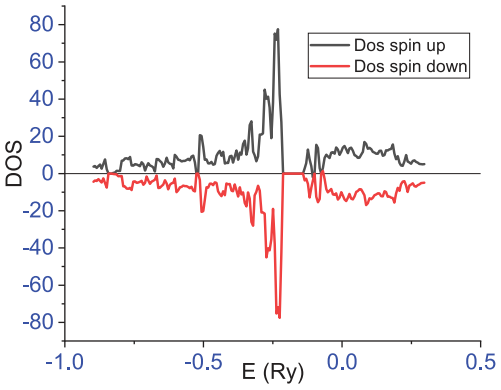

Fig. 10. The density of states (DOS) of the doping of graphite for a concentration equal to $x = 0.01$ of Nickel.

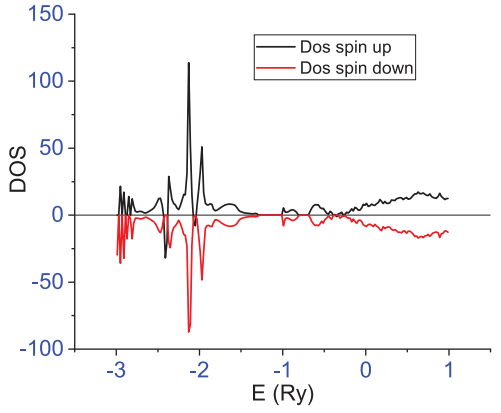

Fig. 11. The density of states (DOS) of the doping of graphite for a concentration equal to $x = 0.40$ of Nickel.

addition. The experimental results about magnetism previously reported in ([29], see Fig. 3) are in accordance with our computed Ni magnetic moment ($0.63\mu_B$) as well since they point out to the measured magnetic moment of about ($0,6\mu_B$).

4.4 Total energy and spin momentum of C_{1-x} Ni_x

The total energy given in Rydberg (Ry) of $C_{1-x}Ni_x$ system points out to a linear variation depending on Ni content x as displayed in Figure 12,

$$E(x)(Ry) = -92.99 \times x - 131.5.$$

The linearity of the data was confirmed by a coefficient of determination $R^2 = 0.987$. The negative slope of the linear model showed that $C_{1-x}Ni_x$ compounds possessed a minimal energies for large x values. Figure 13 shows the evolution of the spin momentum of the $C_{1-x}Ni_x$ compounds as a function of x. As other result, when Ni content x varies from 0 to 0.5, the spin moment of graphite increases, whereas the spin nickel decreases. At x greater than 0.5, we notice that the spin moment of nickel increases while the spin moment of graphite decreases.

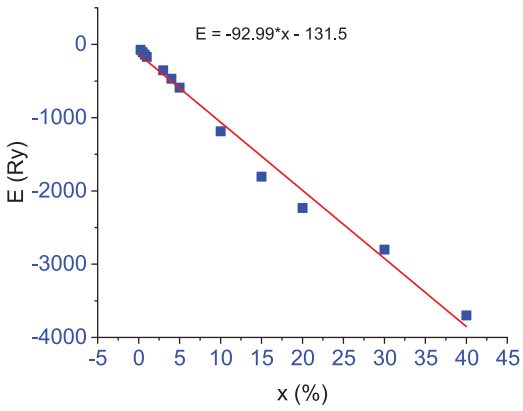

Fig. 12. The linear variation of the computed total energy versus Ni concentration in C-Ni alloy.

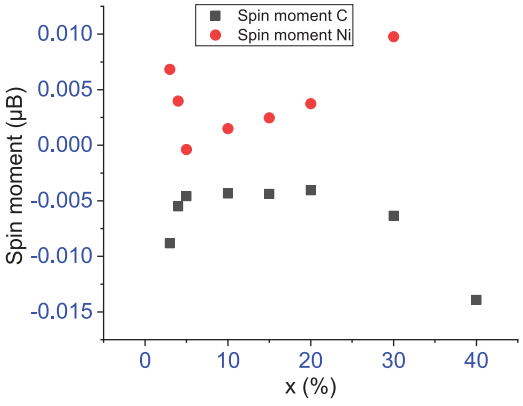

Fig. 13. The variation of the spin moment of graphite and Nickel versus the Ni content in C-Ni alloy.

5 Conclusion

The presence of nickel atoms in the disordered interstitial sites strongly affects the DOS of graphite. The insertion of Nickel atoms in graphite introduced unoccupied energy levels. We found that graphite, even when its DOS showed more distinctive peaks similar to those of the molecular DOS, recovered its semi-circular character. This was because the charge values in the various bands were comparable to those of pure graphite, and the DOS was continuous in the vicinity of the Fermi level.The magnetization of the graphite decreased when the occupation of the Ni site was almost complete. This was primarily due to the rearrangement between spin-up and spin-down populations when Ni increased.

Author contribution statement

Abdellah Sellam performed all the simulations and wrote and supervised the manuscript. El Kebir Hlil and Rodolphe Heyd helped analyze, interpret and discuss the results. Abdelaziz Koumina helped to improve, analyze and carefully read the document. All authors contributed to the preparation of the manuscript. Also, all authors read and approved the final manuscript.

Appendix A: Density of states according to the ratio (c/a)

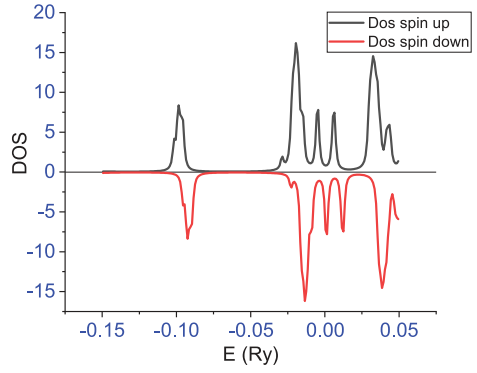

Fig. A.1. ($c/a = 2.560$).

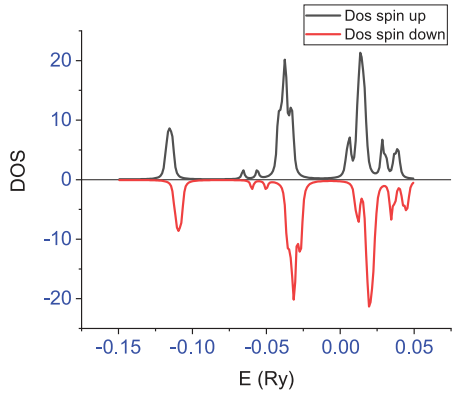

Fig. A.2. ($c/a = 2.580$).

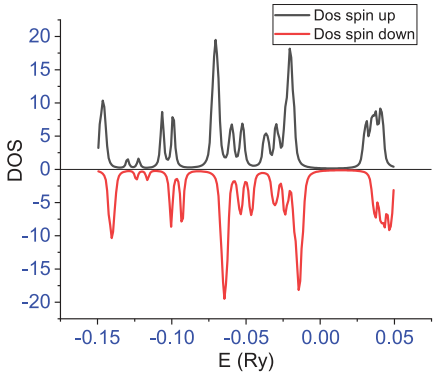

Fig. A.3. ($c/a = 2.621$).

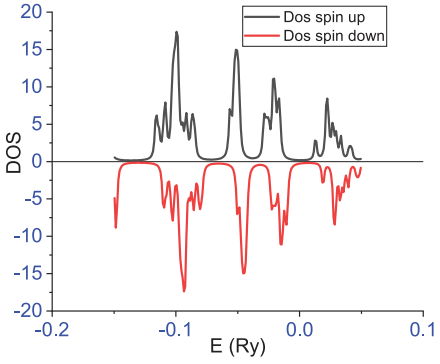

Fig. A.4. ($c/a = 2.662$).

Appendix B: Nickel-doping on graphite

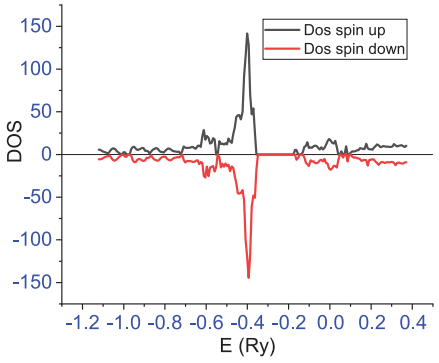

Fig. B.1. Electronic density of states of $C_{95}Ni_5$.

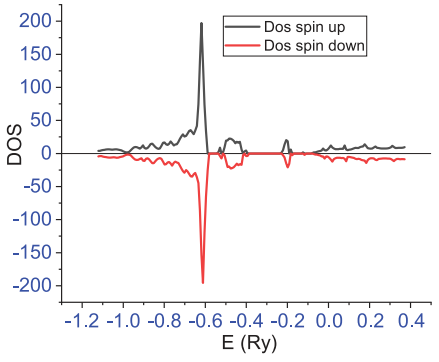

Fig. B.2. Electronic density of states of $C_{90}Ni_{10}$.

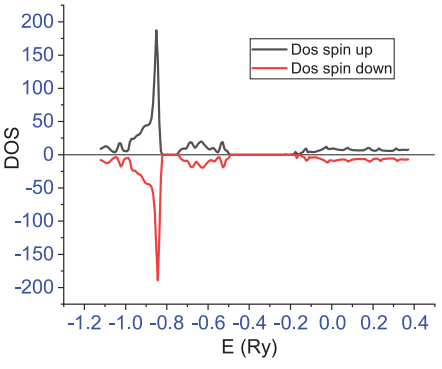

Fig. B.3. Electronic density of states of $C_{85}Ni_{15}$.

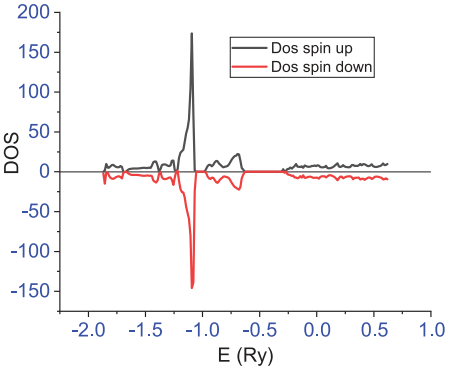

Fig. B.4. Electronic density of states of $C_{80}Ni_{20}$.

References

1. R.M. Torres-Rojas, R. Baquero, Carbon **21**, 11052 (2016)
2. P. Hohenberg, W. Kohn, Phys. Rev. B **136**, 864 (1964)
3. W. Kohn, L.J. Sham, Phys. Rev. A **140**, 1133 (1965)
4. G.K.H. Madsen, P. Blaha, K. Schwarz, E. Sjöstedt, L. Nordström, Phys. Rev. B **64**, 19 (2001)
5. P. Blaha, K. Schwarz, G.K.H. Madsen, D. Kvasnicka, J. Luitz, WIEN2K, An Augmented Plane Wave + Local Orbitals Program for Calculating Crystal Properties, Karlheinz Schwarz, Techn. Universität Wien, Austria, (2013)
6. J.P. Perdew, Y. Wang, Phys. Rev. B **45**, 23 (1992)
7. J.P. Perdew, K. Burke, M. Ernzerhof, Phys. Rev. Lett. **77**, 18 (1996)
8. J.D. Bernal, Proc. R. Soc. London, Ser. A **106**, 740 (1924)
9. R.W.G. Wyckoff, *Crystal Structures*, 2nd edn. Vol. 1 (John Wiley and Sons, New York, 1963)
10. Y. Baskin, L. Meyer, Phys. Rev. **100**, 2 (1955)
11. P. Mavropoulos, N. Papanikolaou, Comput. Nanosci. **31**, 1 (2006)
12. N. Omari, Ph.D. thesis, Faculty of Sciences-Aïn Chock Casa Morocco, 2013
13. Á. Nagy, Phys. Rep. **298**, 1 (1998)
14. H. Akai, J. Phys.: Condens. Matter **1**, 8045 (1989)
15. A.D. Becke, Phys. Rev. A **38**, 3098 (1988)
16. H. Akai, MACHIKANEYAMA2002v08, Departement of Physics, Graduate School of Science, Osaka University, Machikaneyama 1-1, Toyonaka 560-0043, Japan, 2008
17. V.L. Mouruzzi, J.F. Janak, A.R. Williams, *Properties of Metals* (Pergamum, New York, 1998)
18. J.-C. Charlier, J.-P. Michenaud, Phys. Rev. B **46**, 8 (1992)
19. J.N. Decarpigny, Appl. Phys. J. **15**, 3 (1980)
20. R. Heyd, A. Charlier, E. McRae, Phys. Rev. B **55**, 6820 (1997)
21. J.C. Charlier, X. Gonze, J.-P. Michenaud, Phys. Rev. B **43**, 6 (1991)
22. X. Gonze, R. Stumpf, M. Scheffler, Phys. Rev. B **44**, 16 (1991)
23. J.C. Phillips, L. Kleinman, Phys. Rev. **116**, 287 (1959)
24. M.S. Dresselhaus, G. Dresselhaus, K. Sugihara, I.L. Spain, H.A. Goldberg, Springer Ser. Mater. Sci. **5**, 12 (1988)
25. Y. Baskin, L. Mayer, Phys. Rev. **100**, 544 (1955)
26. A.P. Durajski, A.E. Auguscik, R. Szczęśniak, Physica E **119**, 113985 (2020)
27. G. Teobaldi, H. Ohnishi, K. Tanimura, A.L. Shluger, Carbon **48**, 4145 (2010)
28. M.C. Cadeville, C. Lerner, Philos. Mag. **33**, 801 (1976)
29. M.C. Cadeville, C. Lerner, J.M. Friedt, Physica B+C **86–88**, 432 (1977)

Cite this article as: Abdellah Sellam, El Kebir Hlil, Rodolphe Heyd, Abdelaziz Koumina, An ab initio investigation of the electronic and magnetic properties of graphite and nickel-doped graphite, Eur. Phys. J. Appl. Phys. **94**, 10401 (2021)